Electronic Supplementary Material (ESI) for Energy & Environmental Science.

Supporting Information

Hierarchically Stabilized Pt Single-Atom Catalysts Induced by Atomic Substitution Strategy for Efficient Hydrogen Evolution Reaction

Changle Yue,[a] Chao Feng,[a] Guangxun Sun,[a] Na Liu,[a] Haoyuan Hao,[a] Wenjing Bao,[a] Xiaowei Zhang,[a] Fengyue Sun,[a] Cong Zhang,[a] Jiahui Bi,[a] Yan Zhou,[a] Hsiao-Chien Chen,[b] Yuan Pan,[a] Daofeng Sun,[a] and Yukun Lu,*[a]*

*Corresponding author: Yuan Pan, panyuan@upc.edu.cn; Yukun Lu, lyk@upc.edu.cn

Supplementary Text

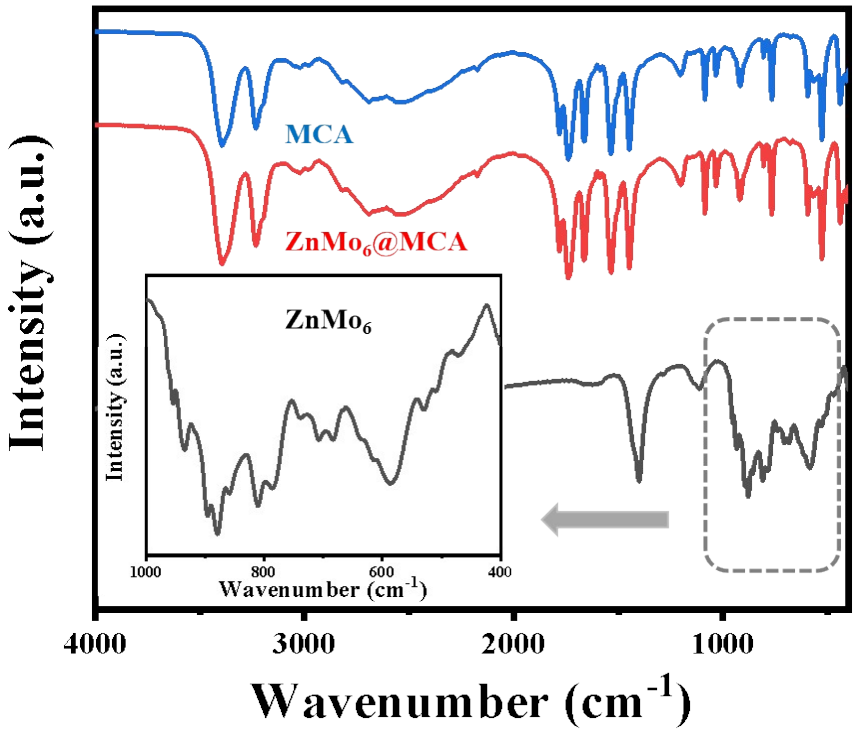

Fig. S1. FT-IR spectra of $ZnMo_6$ (dark gray), MCA (blue) and $ZnMo_6$@MCA (red).

As shown in Fig. S1, the MCA was successfully obtained and maintained in $ZnMo_6$@MCA. The IR characteristic peaks of $ZnMo_6$ were not exhibited in $ZnMo_6$@MCA, which may be due to the low content of $ZnMo_6$ resulting in the masking of the characteristic peaks below 1000 cm^{-1}.

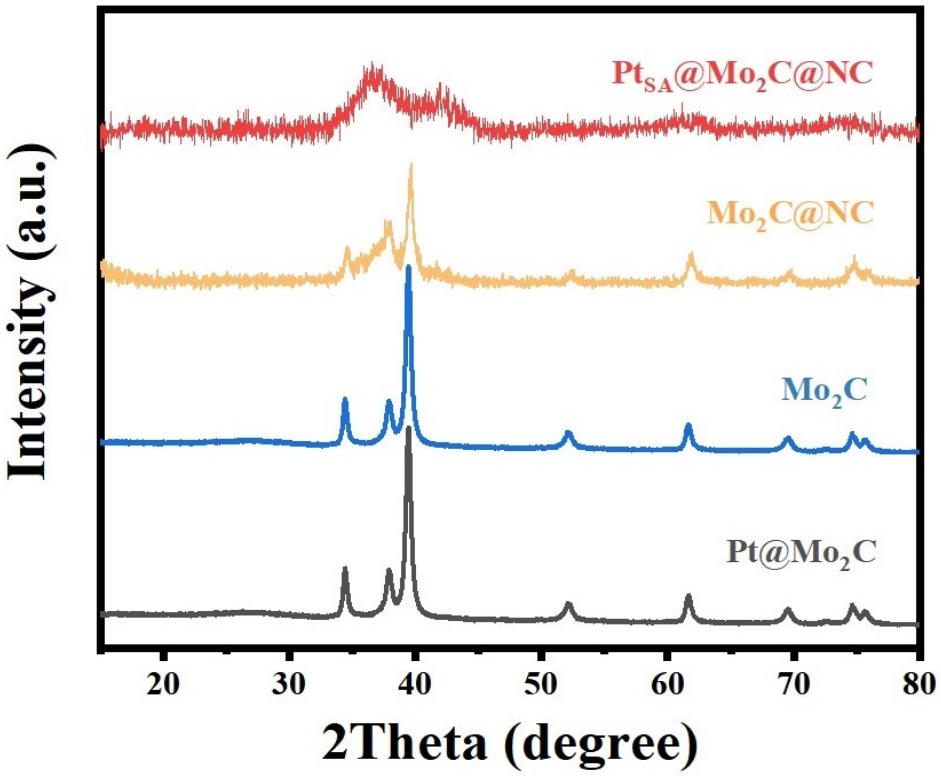

Fig. S2. XRD patterns for $Pt_{SA}@Mo_2C@NC$, $Mo_2C@NC$, Mo_2C and $Pt@Mo_2C$.

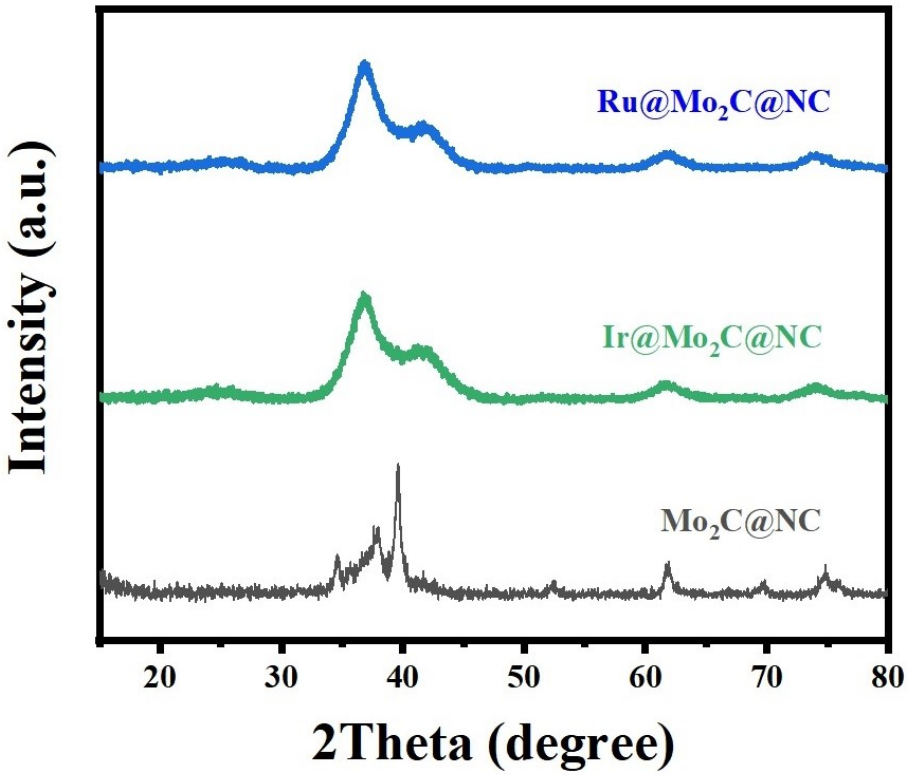

Fig. S3. XRD patterns for Ru@Mo_2C@NC, Ir@Mo_2C@NC and Mo_2C@NC.

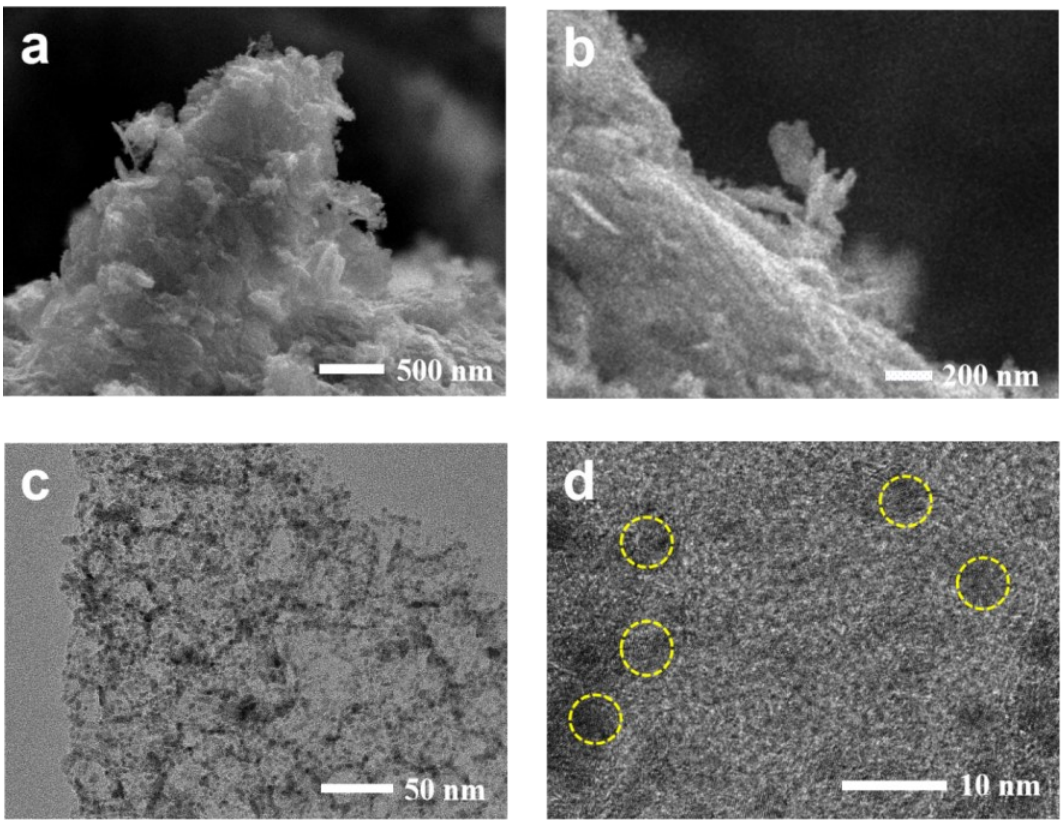

Fig. S4. Morphology and structure of Pt_{SA}@Mo_2C@NC. (a, b) SEM images of Pt_{SA}@Mo_2C@NC and (c, d) HRTEM images of Pt_{SA}@Mo_2C@NC.

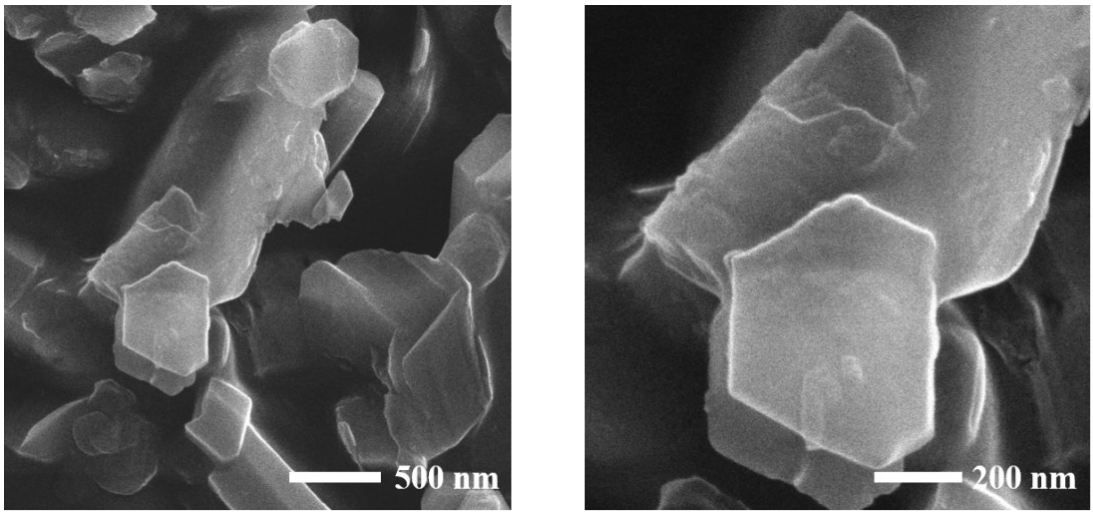

Fig. S5. SEM image of $ZnMo_6$@MCA.

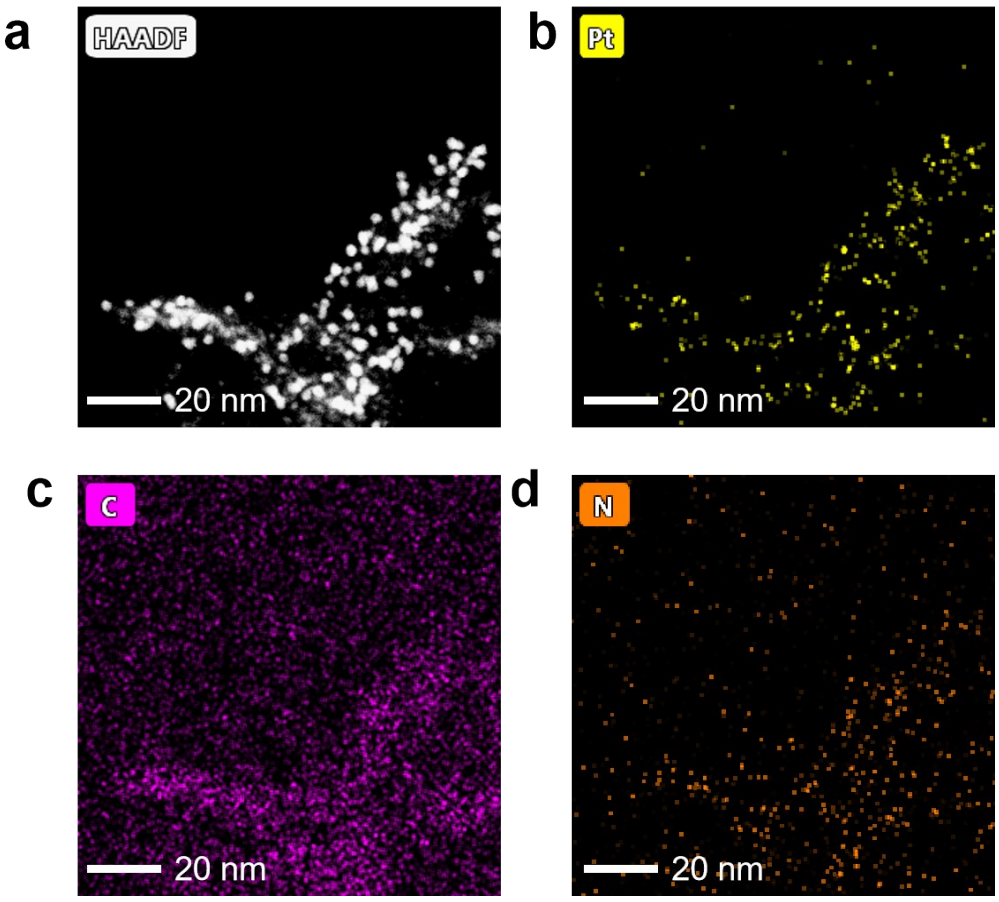

Fig. S6. HAADF-STEM images of Pt, C and N elements in Pt@NC.

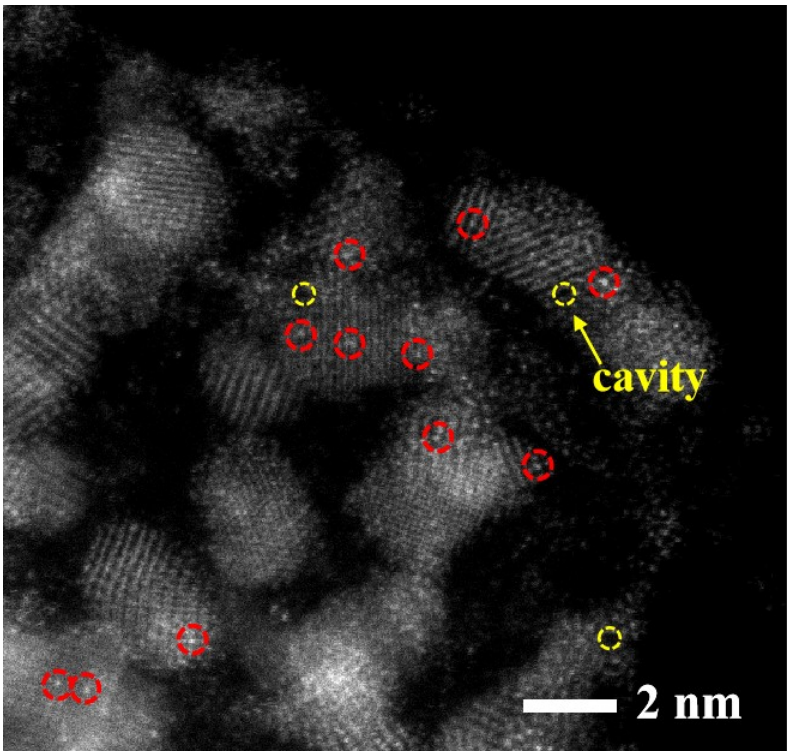

Fig. S7. AC-HAADF-STEM image of Pt_{SA}@Mo_2C@NC.

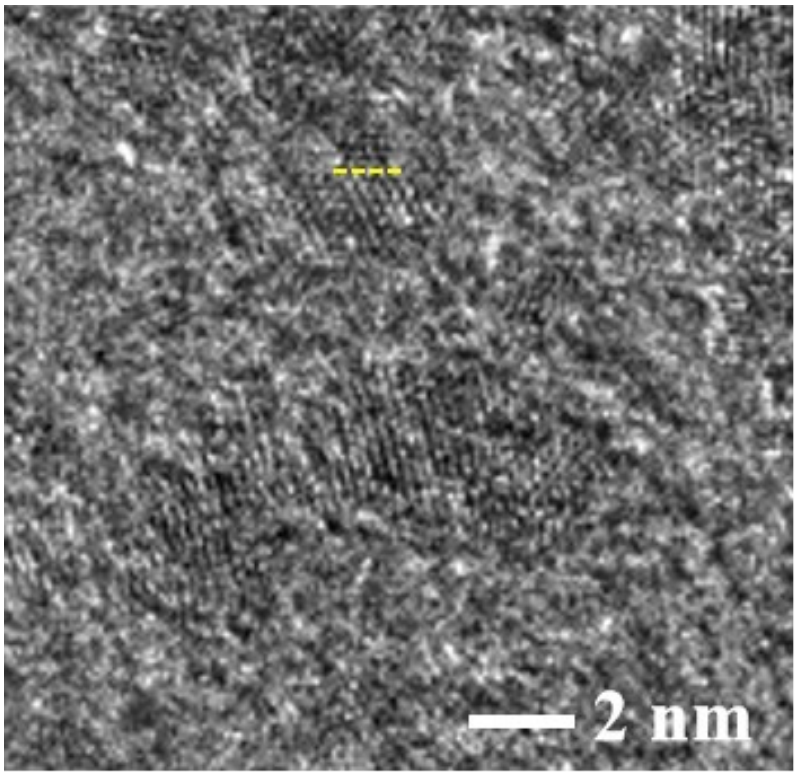

Fig. S8. Schematic HRTEM of Mo_2C@NC: the yellow line corresponds to the intensity map of Mo_2C in Fig. 3f of the manuscript.

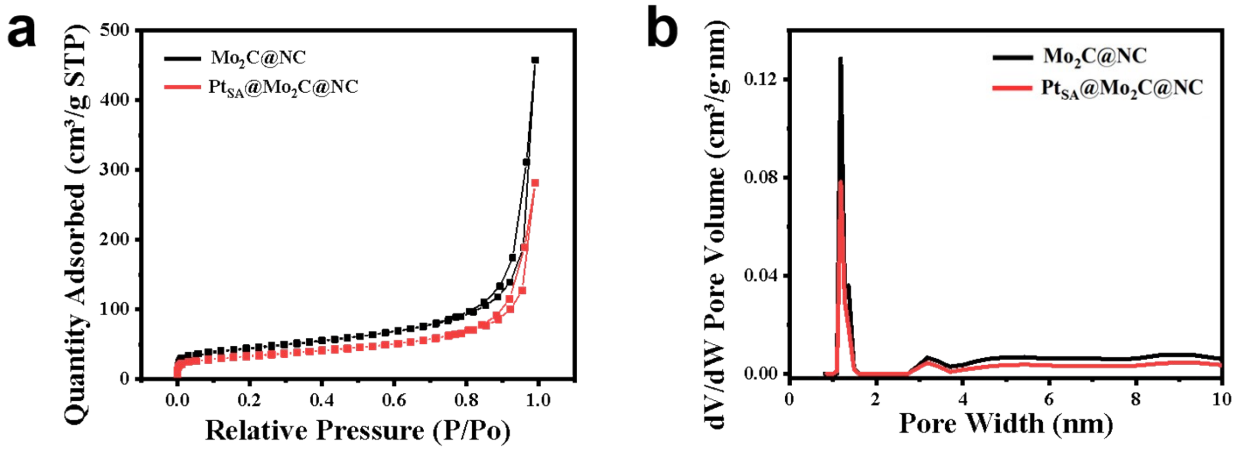

Fig. S9. Apparent structure of $Pt_{SA}@Mo_2C@NC$. (a) Nitrogen adsorption-desorption isotherms and (b) DFT pore distribution of $Pt_{SA}@Mo_2C@NC$ and $Mo_2C@NC$

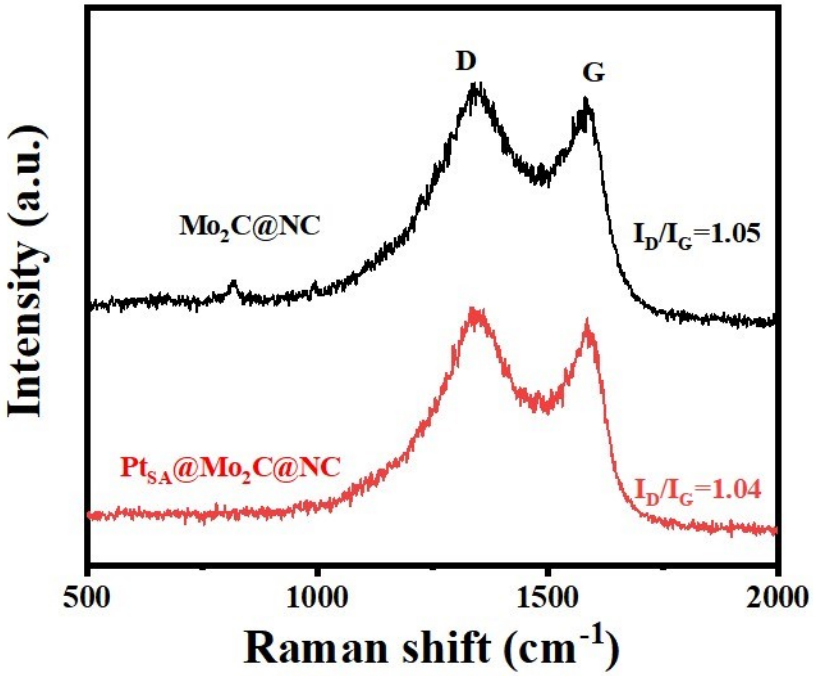

Fig. S10. Raman spectrum of Pt_{SA}@Mo_2C@NC and Mo_2C@NC.

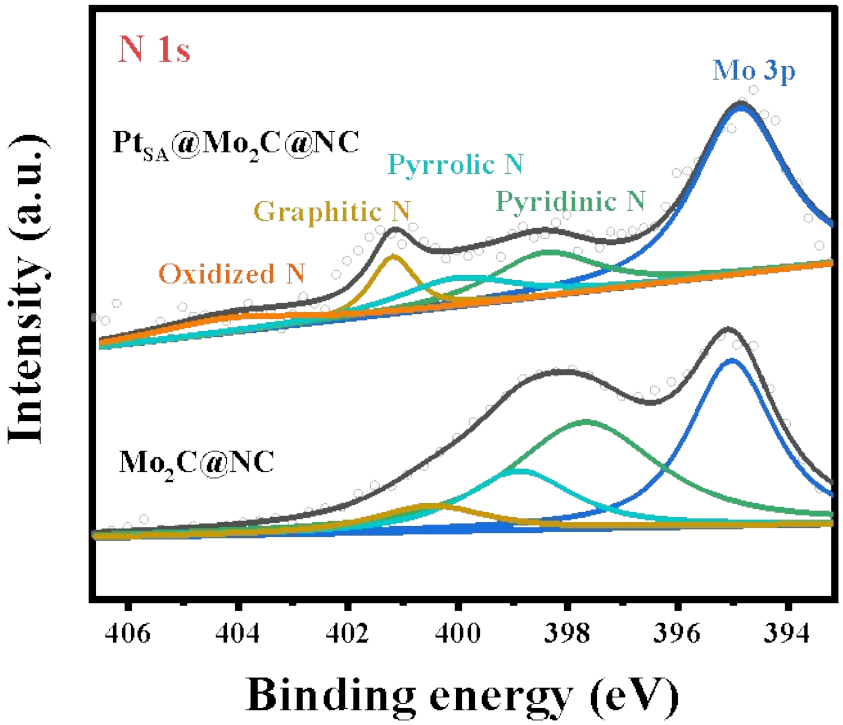

Fig. S11. High-resolution XPS spectra of N 1s in Pt_{SA}@Mo_2C@NC and Mo_2C@NC.

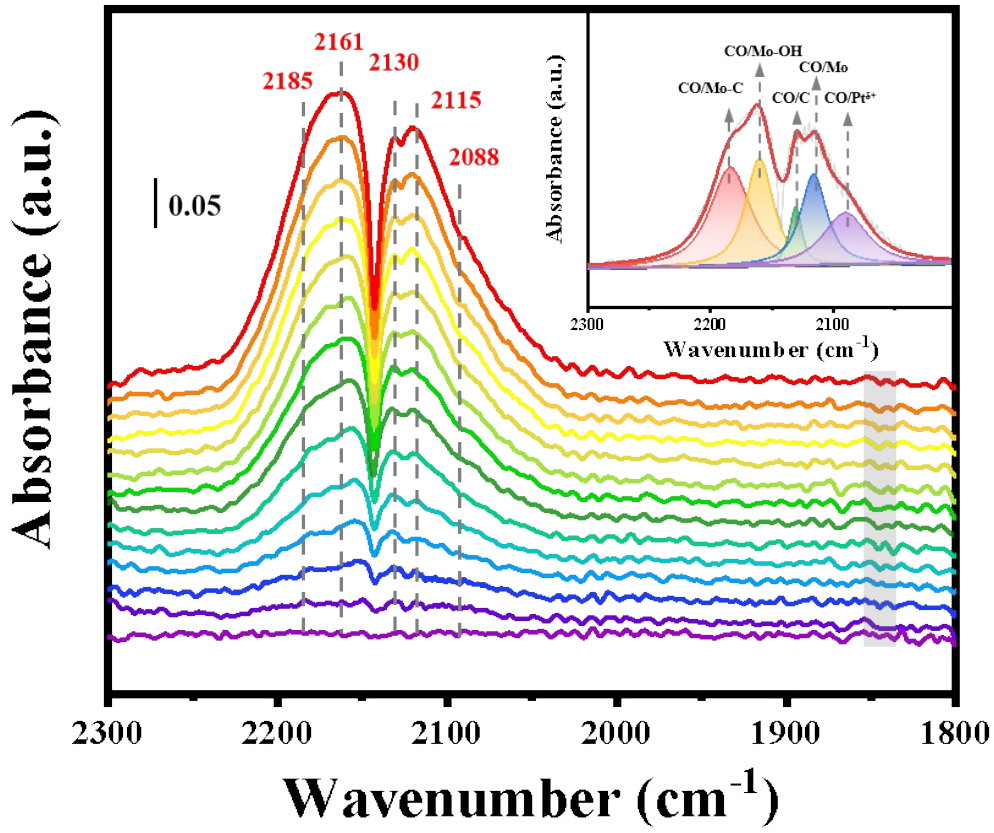

Fig. S12. IR/CO spectra and decomposition of the saturated CO adsorption spectra (inset) of $Pt_{SA}@Mo_2C@NC$

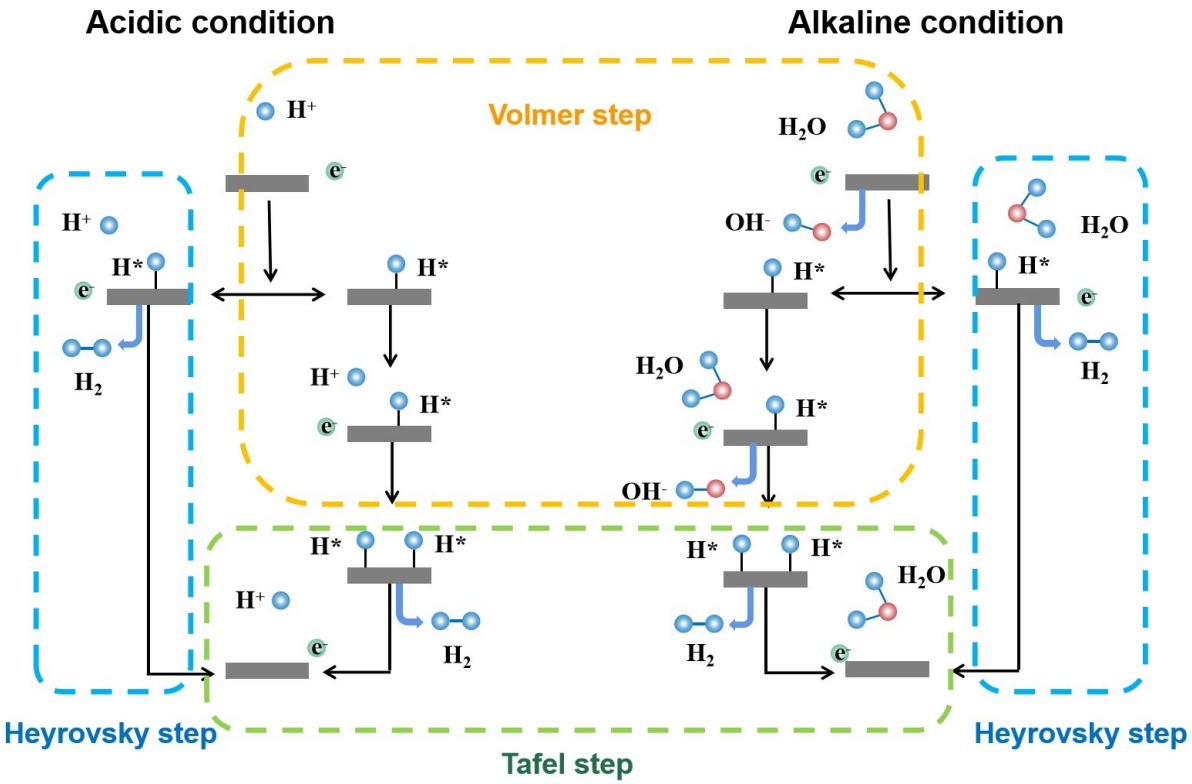

Fig. S13. Schematic representation of the HER mechanism under acidic and alkaline conditions.

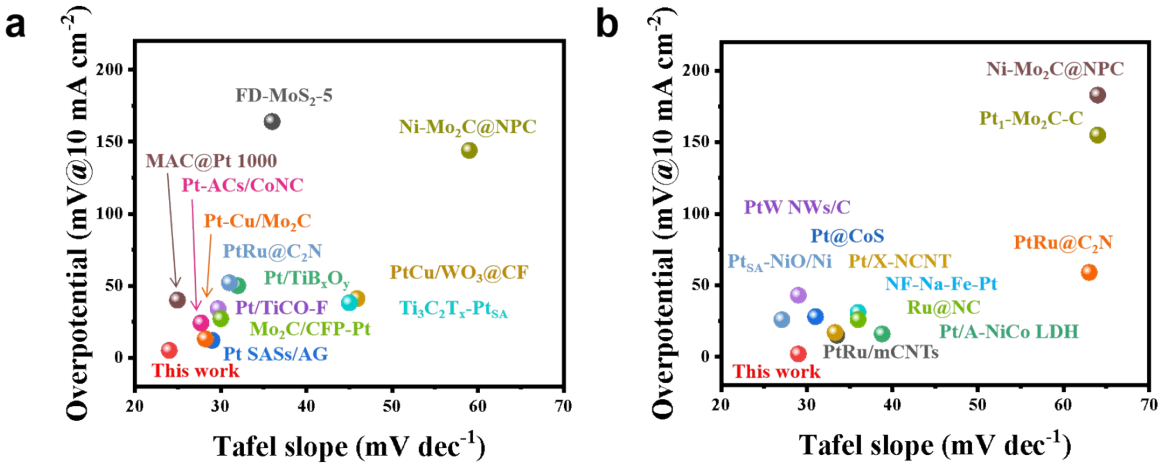

Fig. S14. HER performance comparison of reported catalysts. Comparison graph of catalyst performance in (a) 0.5 M H_2SO_4 and (b) 1.0 M KOH: including overpotential and Tafel slope.

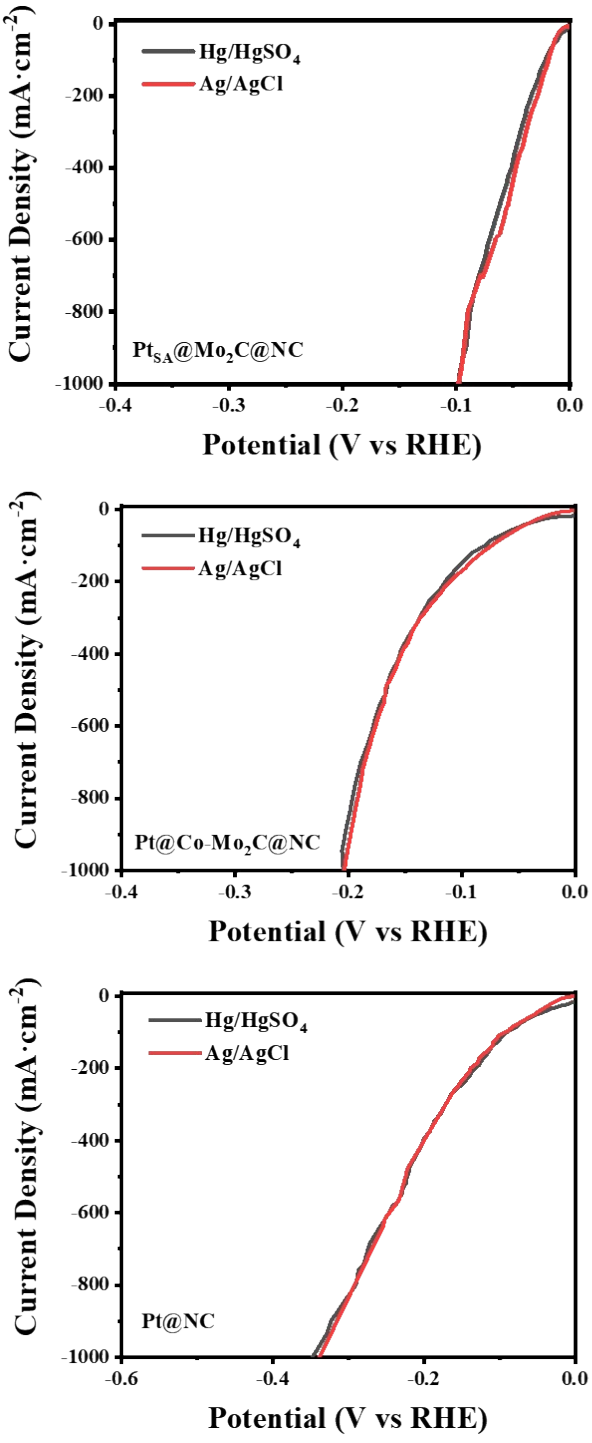

Fig. S15. Polarization curves of HER in 0.5 M H_2SO_4 of Pt_{SA}@Mo_2C@NC, Pt@Co-Mo_2C@NC, Pt@NC using the $Hg/HgSO_4$ reference electrode.

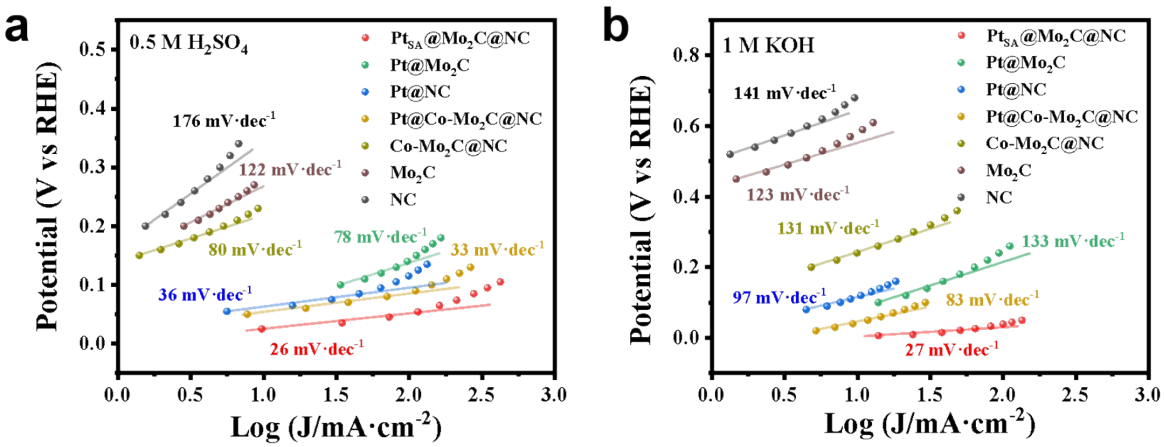

Fig. S16. Tafel curve of series catalysts. Tafel curves of various catalysts of Pt_{SA}@Mo_2C@NC, Pt@Mo_2C, Pt@NC, Co-Mo_2C@NC, Mo_2C@NC and NC in (a) 0.5 M H_2SO_4 and (b) 1.0 M KOH measured by the controlled potential electrolysis.

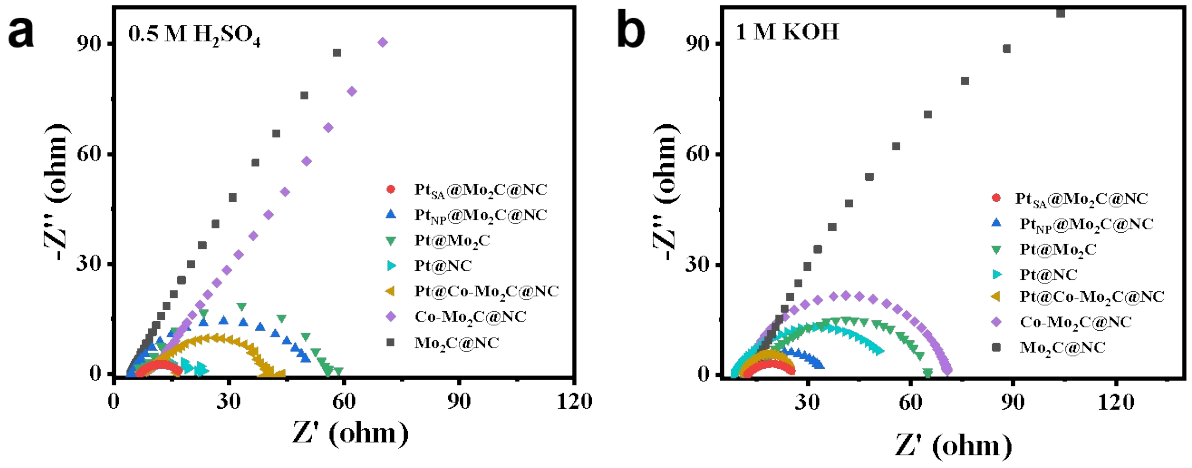

Fig. S17. Resistances of series catalysts. Electrochemical impedance spectroscopy (EIS) of of Pt_{SA}@Mo_2C@NC, Pt@Mo_2C, Pt@NC, Co-Mo_2C@NC, Mo_2C@NC and NC in (a) 0.5 M H_2SO_4 and (b) 1.0 M KOH.

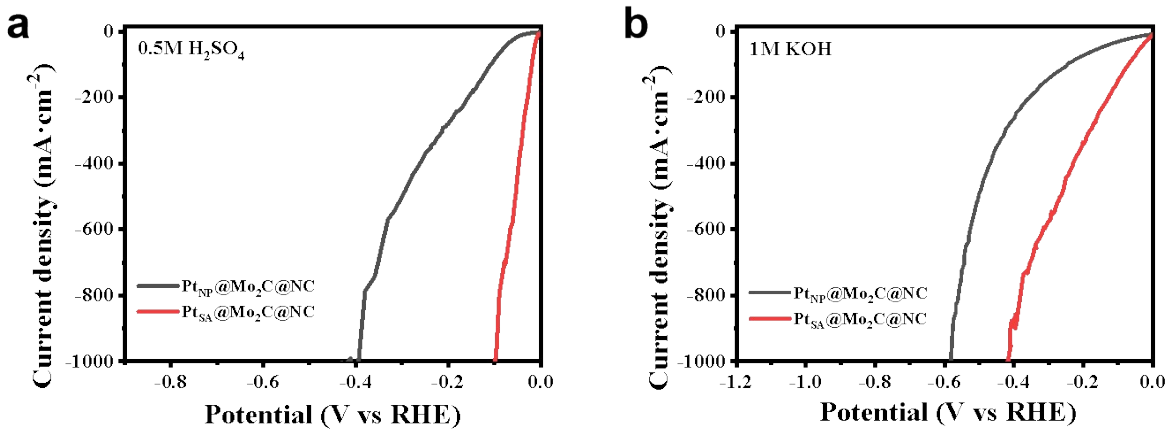

Fig. S18. HER performance of Pt_{NP}@Mo_2C@NC and Pt_{NP}@Mo_2C@NC. HER polarization curves of Pt_{SA}@Mo_2C@NC and Pt_{NP}@Mo_2C@NC in 0.5 M H_2SO_4 (a) and 1.0 M KOH (b).

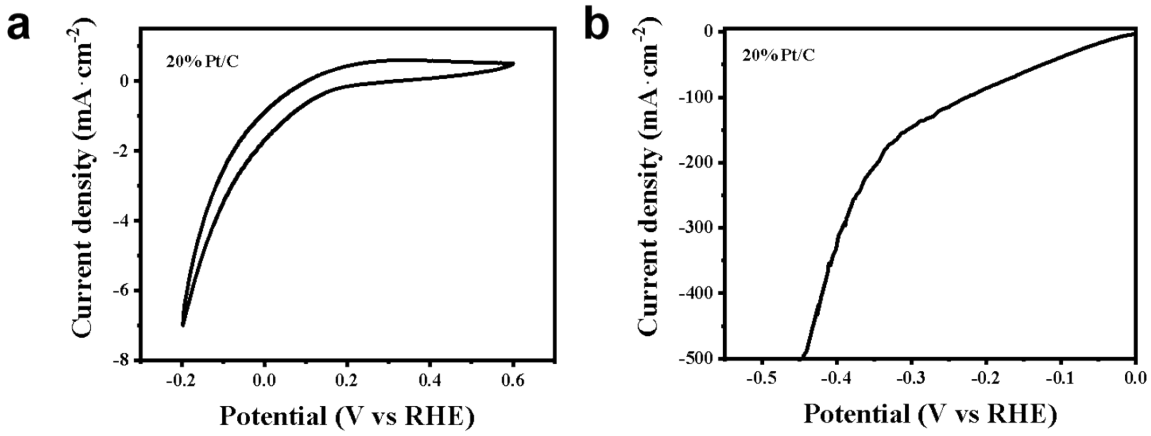

Fig. S19. Performance of commercial 20% Pt/C. (a) CV curve in 1.0 M PBS solution and (b) LSV curve in 0.5 M H_2SO_4 of 20% Pt/C catalyst.

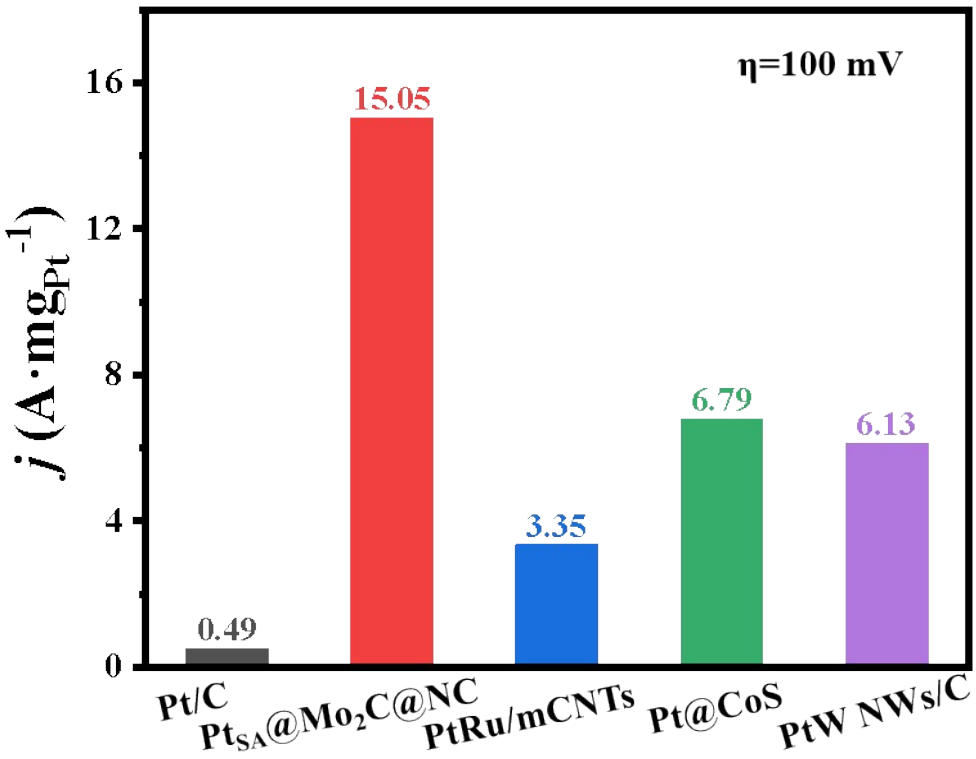

Fig. S20. Mass activity of Pt_{SA}@Mo_2C@NC catalyst and other reported catalysts in 1.0 M KOH.

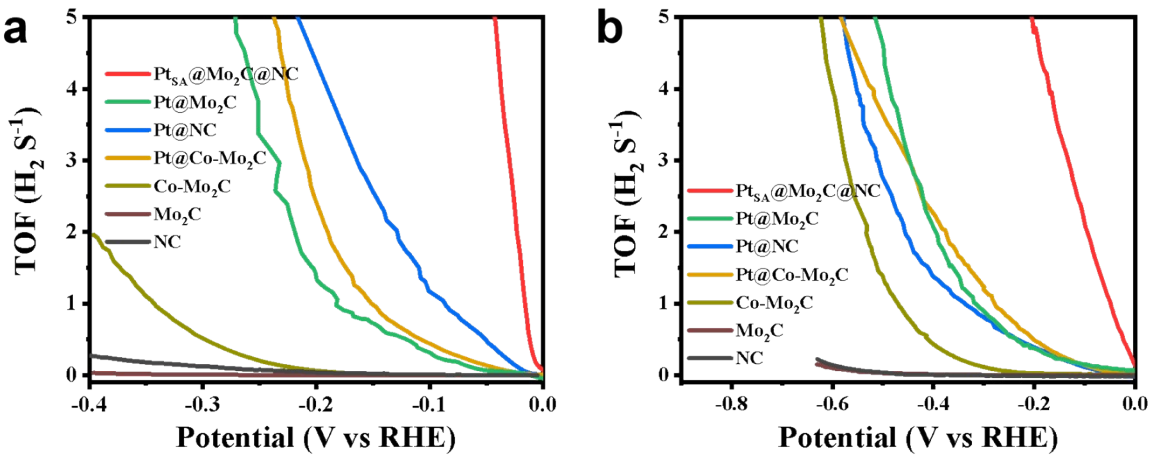

Fig. S21. Intrinsically active of series catalysts. Turnover frequency (TOF) of the catalysts tested in 0.5 M H_2SO_4 (a) and 1M KOH (b) solution.

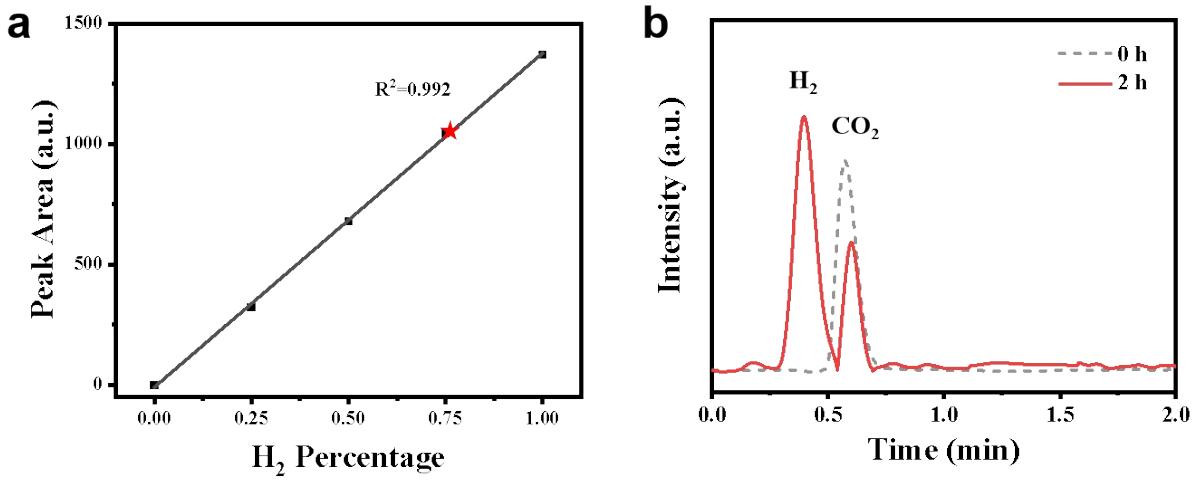

Fig. S22. (a) The calibration curve obtained by ultrapure hydrogen (99.999%) and (b) gas chromatogram before and after electrolysis.

The calibration curve was obtained using ultrapure hydrogen (99.999%) of different concentrations in Fig. S22a. CO_2 is used to displace the air inside the cathode electrolytic cell. The 1 mL gas above the electrolyte was then analysed by gas chromatography, as shown in Fig. S22b. After the electrolysis of the Pt_{SA}@Mo_2C@NC catalyst under a current of 100 mA·cm^{-2} for 2 h, the 1 mL gas mixture above the electrolyte was taken from the cathodic electrolytic cell and analysed by gas chromatography. Then, applying the dilution factor, it was possible to know the amount of hydrogen present in the Head Space. The red mark in Fig. 22a indicates that the amount of hydrogen in the mixed gas after electrolysis is about 0.752 mL.

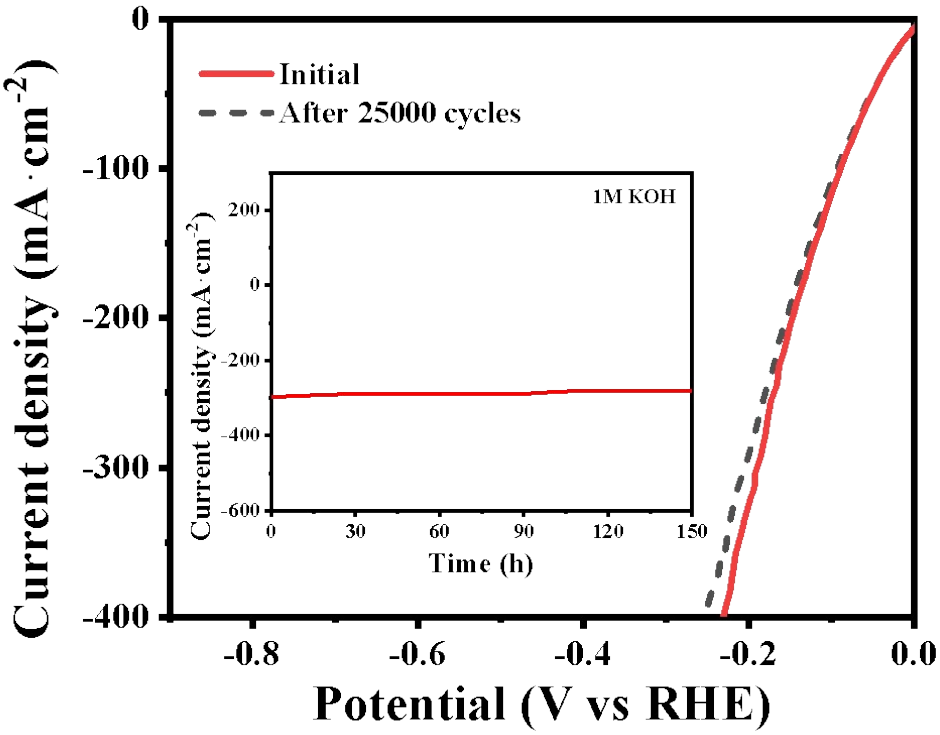

Fig. S23. Stability test of Pt_{SA}@Mo_2C@NC in 1.0 M KOH.

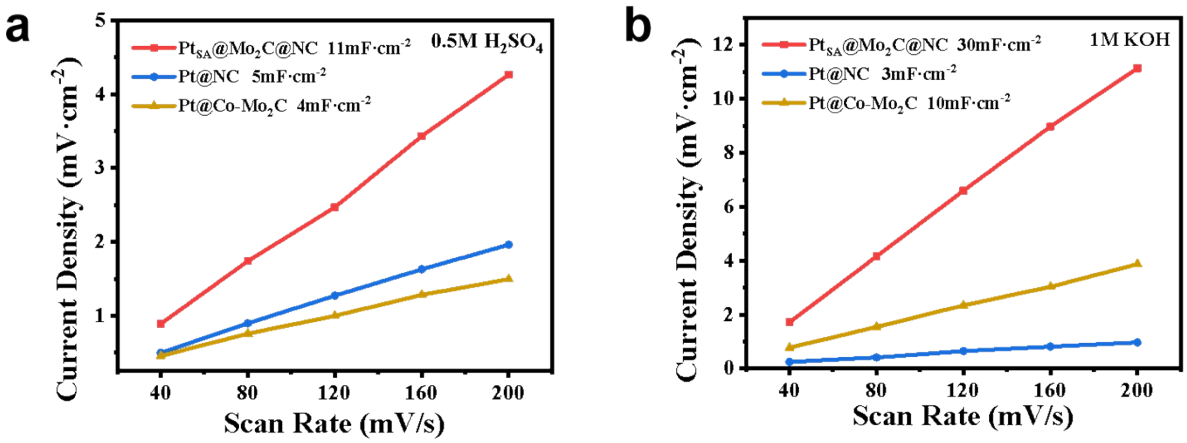

Fig. S24. Double-layer capacitance (C_{dl}) of series catalysts. C_{dl} determined by plotting capacitive currents as function of scan rate in of alkaline (a) and acidic solutions (b).

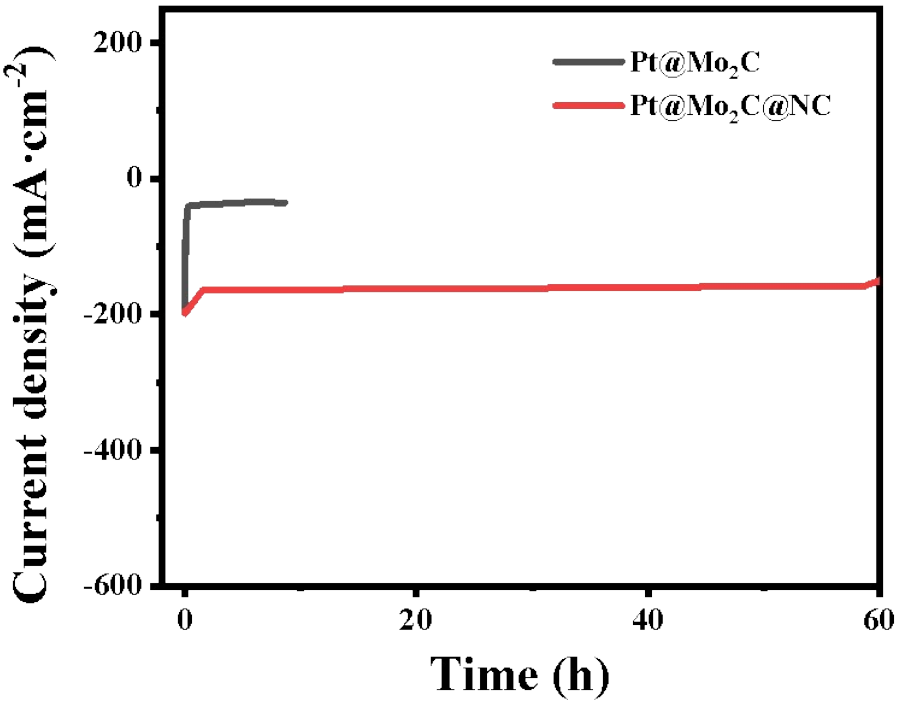

Fig. S25. Stability test of Pt_{SA}@Mo_2C@NC and Pt@Mo_2C.

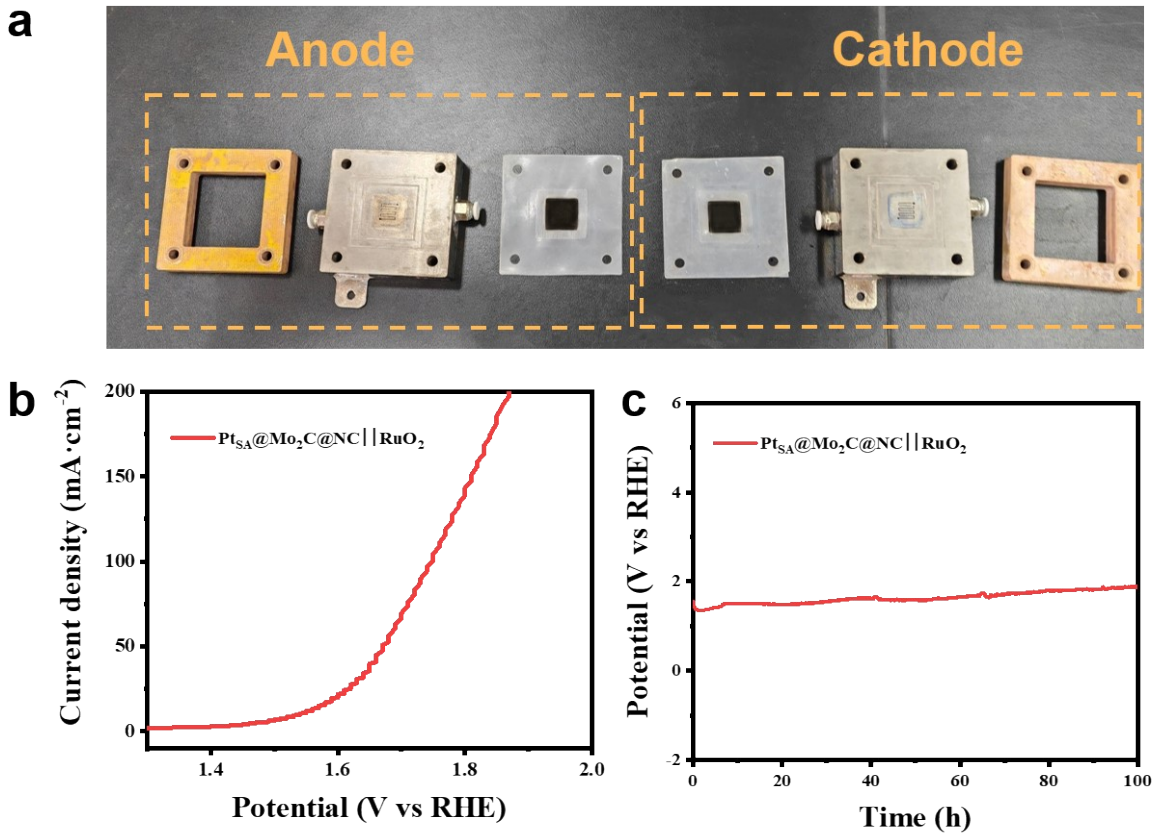

Fig. S26. (a) Photograph of the PEM device, (b) the polarization curves of Pt_{SA}@Mo_2C@NC recorded between 1.3 and 2.0 V_{cell} at 50 °C in neutral solution. (c)The voltage–time stability of Pt_{SA}@Mo_2C@NC as cathode in PEM.

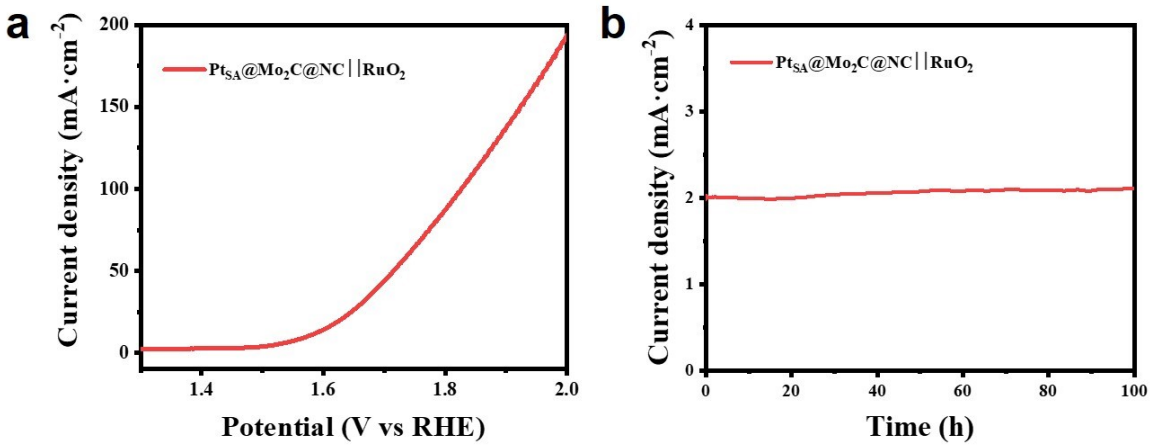

Fig. S27. (a) The polarization curves of $Pt_{SA}@Mo_2C@NC$ recorded between 1.3 and 2.0 V_{cell} at 50 °C in neutral solution. (b)The voltage–time stability of $Pt_{SA}@Mo_2C@NC$ as cathode in AEM.

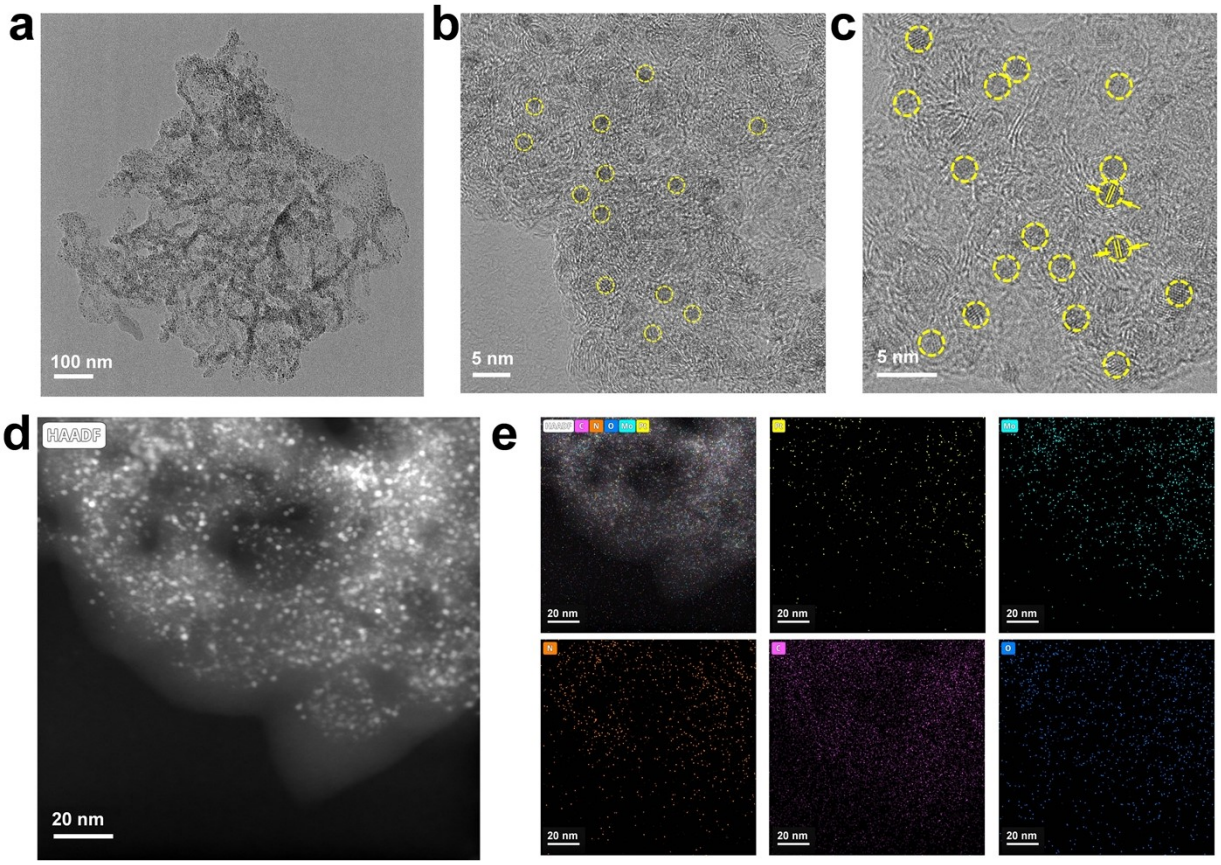

Fig. S28. (a-c) HRTEM and (d) HAADF-STEM images and (e) corresponding EDS mapping of Pt_{SA}@Mo_2C@NC after HER stability test.

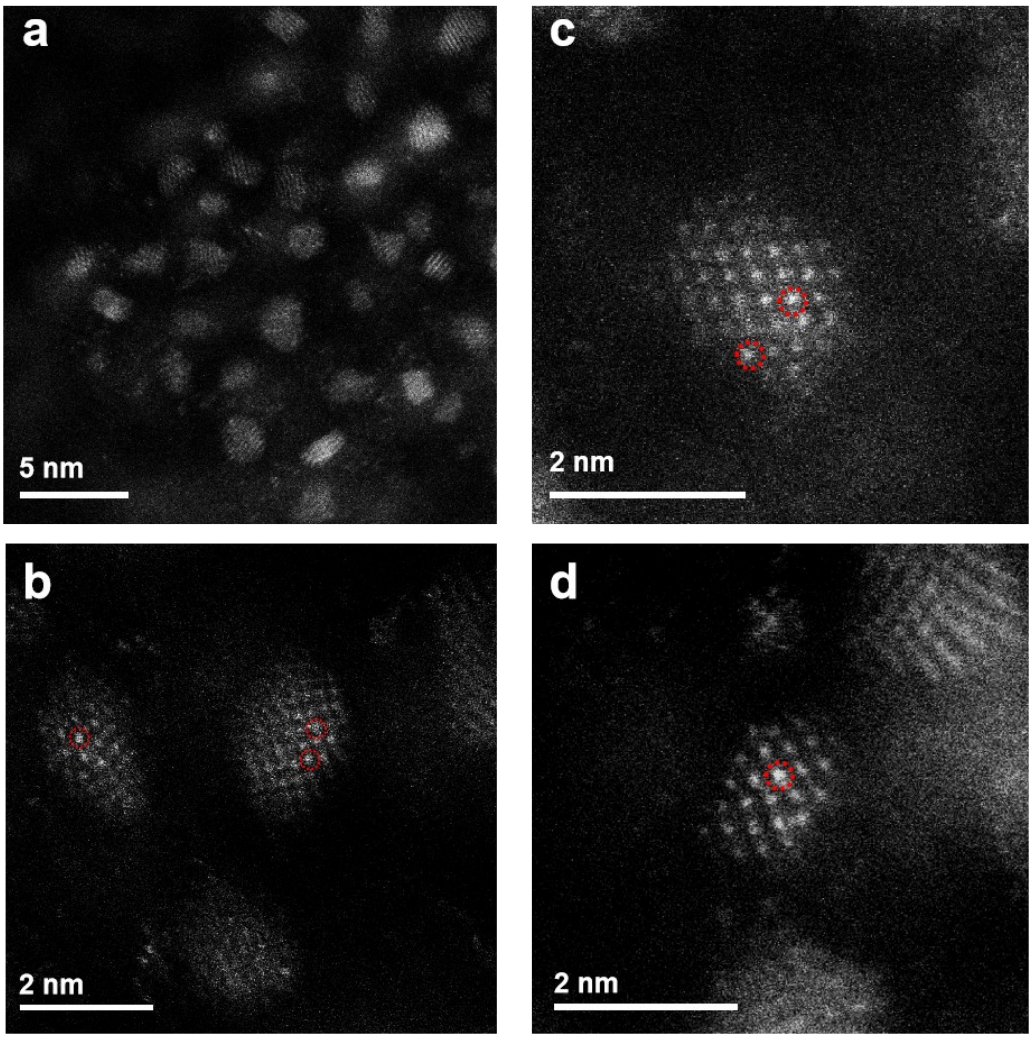

Fig. S29. AC-HAADF-STEM images of Pt_{SA}@Mo_2C@NC after HER process.

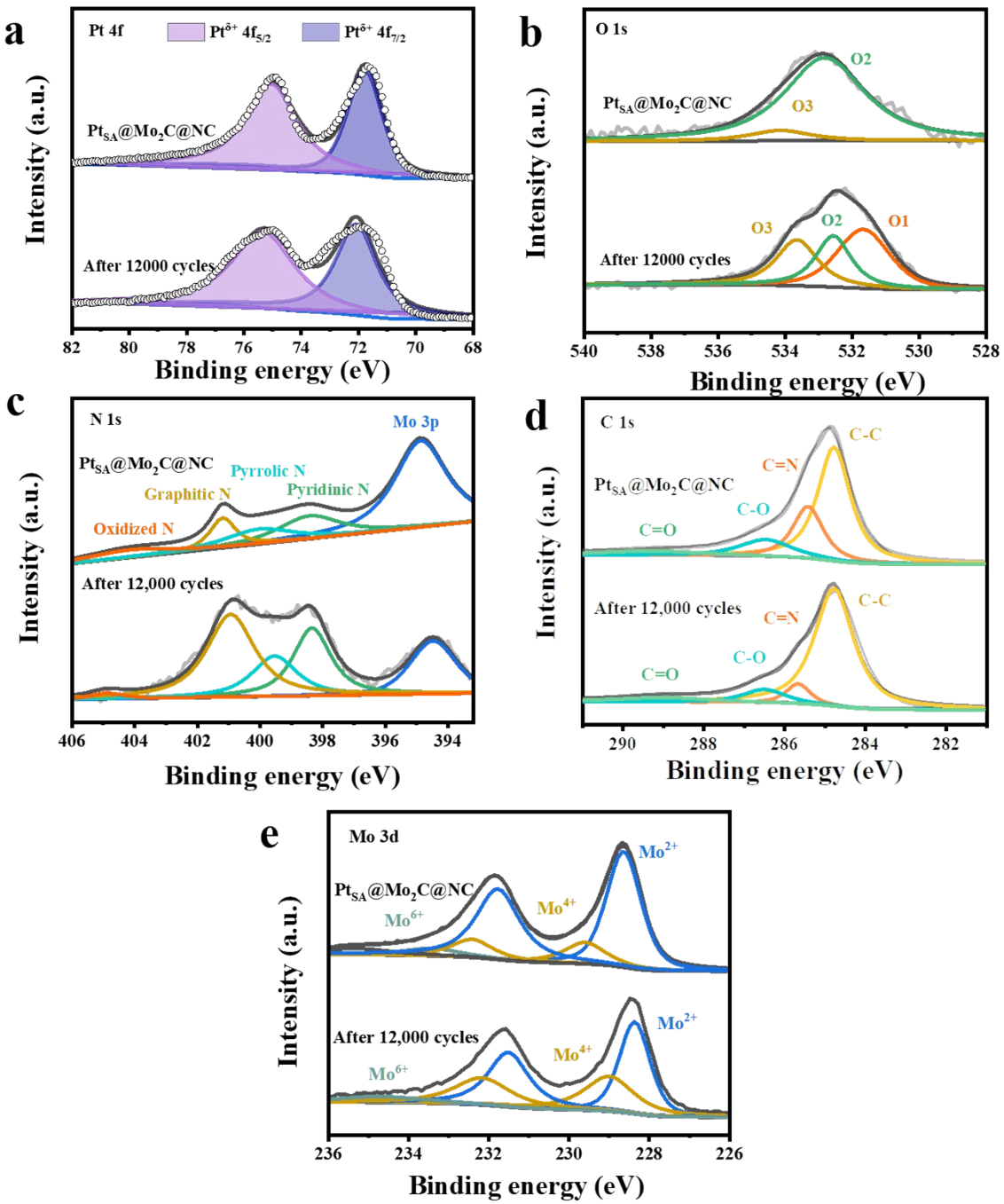

Fig. S30. Electronic structure before and after the HER process. High-resolution XPS spectra of Pt 4f (a), O 1s (b), N 1s (c), C 1s (d) and Mo 3d (e) in pristine $Pt_{SA}@Mo_2C@NC$ and $Pt_{SA}@Mo_2C@NC$ after 12,000 cycles.

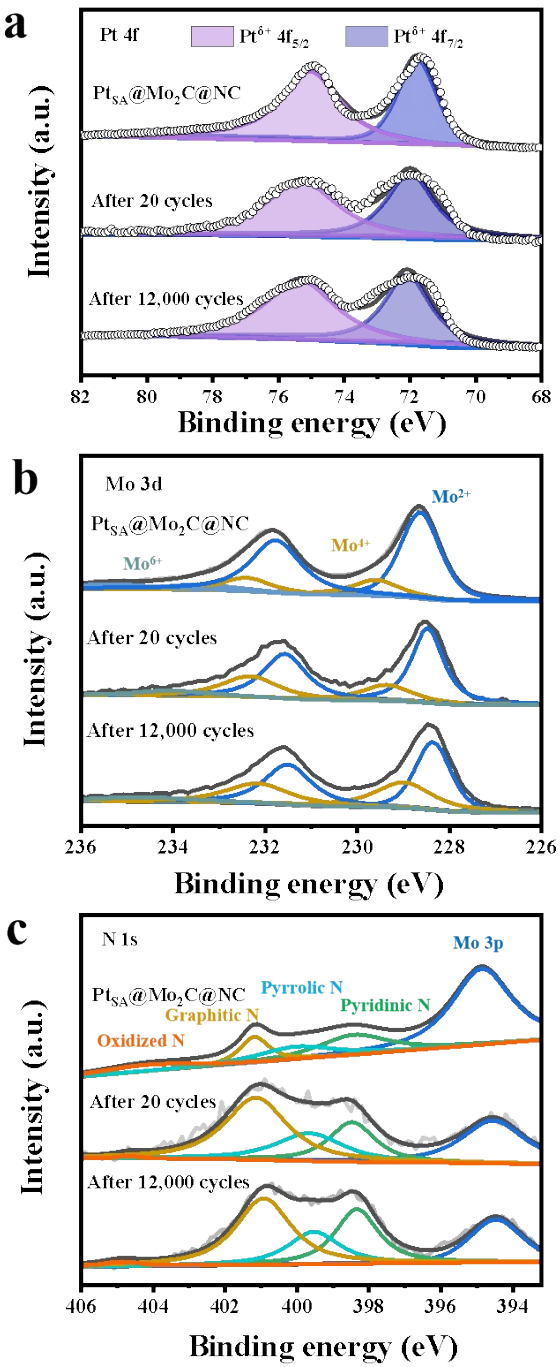

Fig. S31. Electronic structure before and after the HER process. High-resolution XPS spectra of Pt 4f (a), Mo 3d (b) and N 1s (c) in pristine Pt_{SA}@Mo_2C@NC and Pt_{SA}@Mo_2C@NC after 20 and 12,000 cycles.

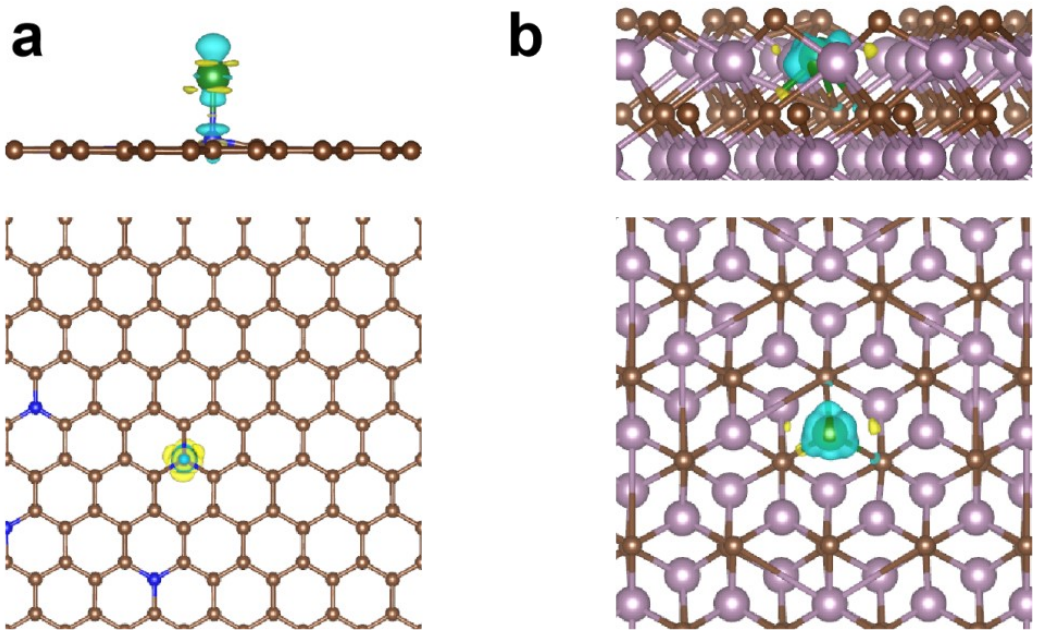

Fig. S32. Charge density difference of Pt@NC (a) and Pt@Mo_2C (b). Pt atoms: green; Mo atoms: purple; N atoms: blue, C atoms: brown.

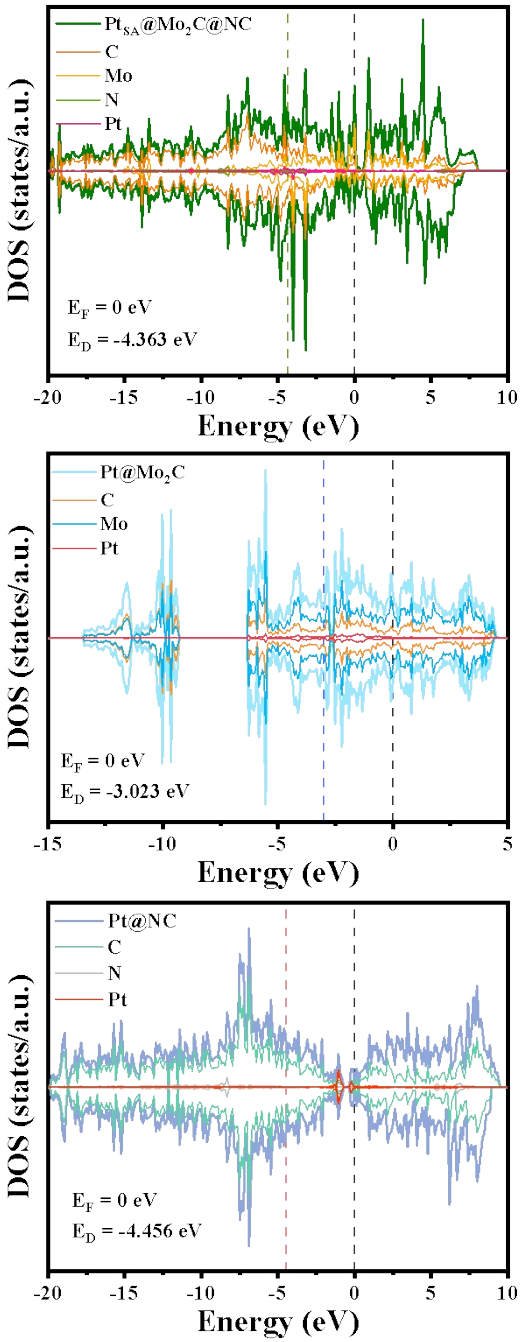

Fig. S33. Schematic of DOS with different elements of Pt_{SA}@Mo_2C@NC, Pt@Mo_2C and Pt@NC.

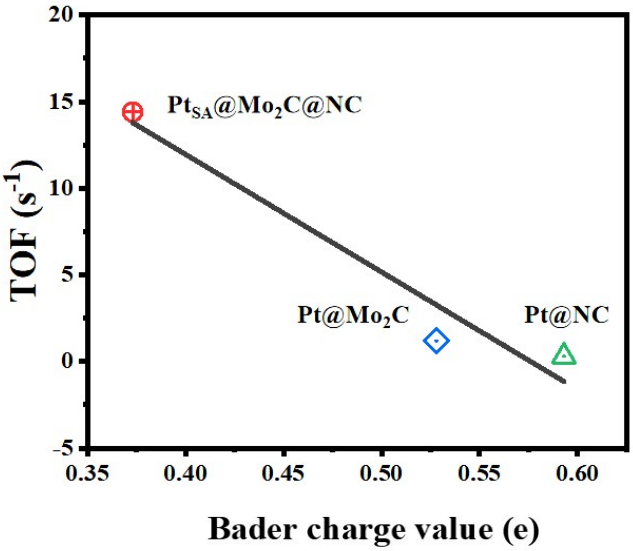

Fig. S34. Linear relationship between Bader charge value and TOF of $Pt_{SA}@Mo_2C@NC$, $Pt@Mo_2C$ and Pt@NC.

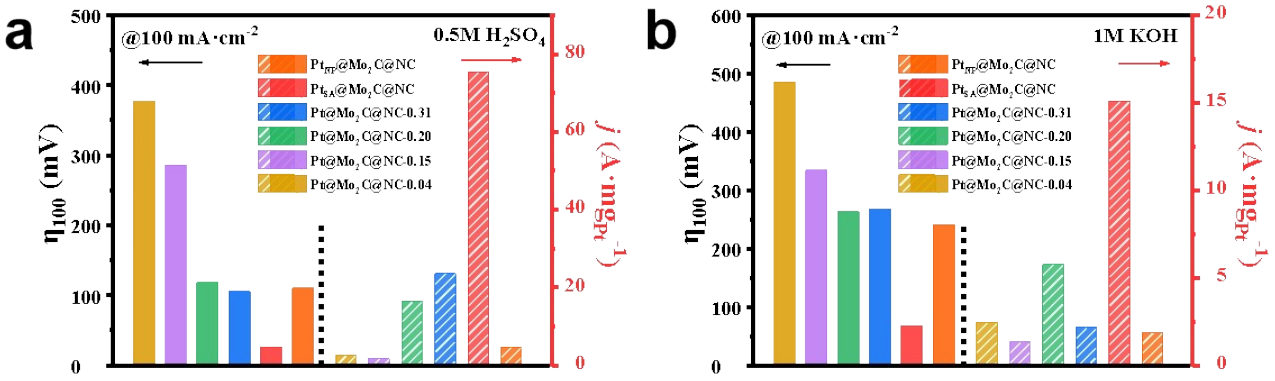

Fig. S35. Pt loading optimization results are plotted for samples with different Pt wt%: Pt_{NP}@Mo_2C@NC (1.05%), Pt_{SA}@Mo_2C@NC (0.94%), Pt@Mo_2C@NC-0.31 (0.31%), Pt@Mo_2C@NC-0.20 (0.20%), Pt@Mo_2C@NC-0.15 (0.15%), Pt@Mo_2C@NC-0.04 (0.04%). Comparative plots of overpoints and mass activity under acidic (A) and alkaline conditions (B).

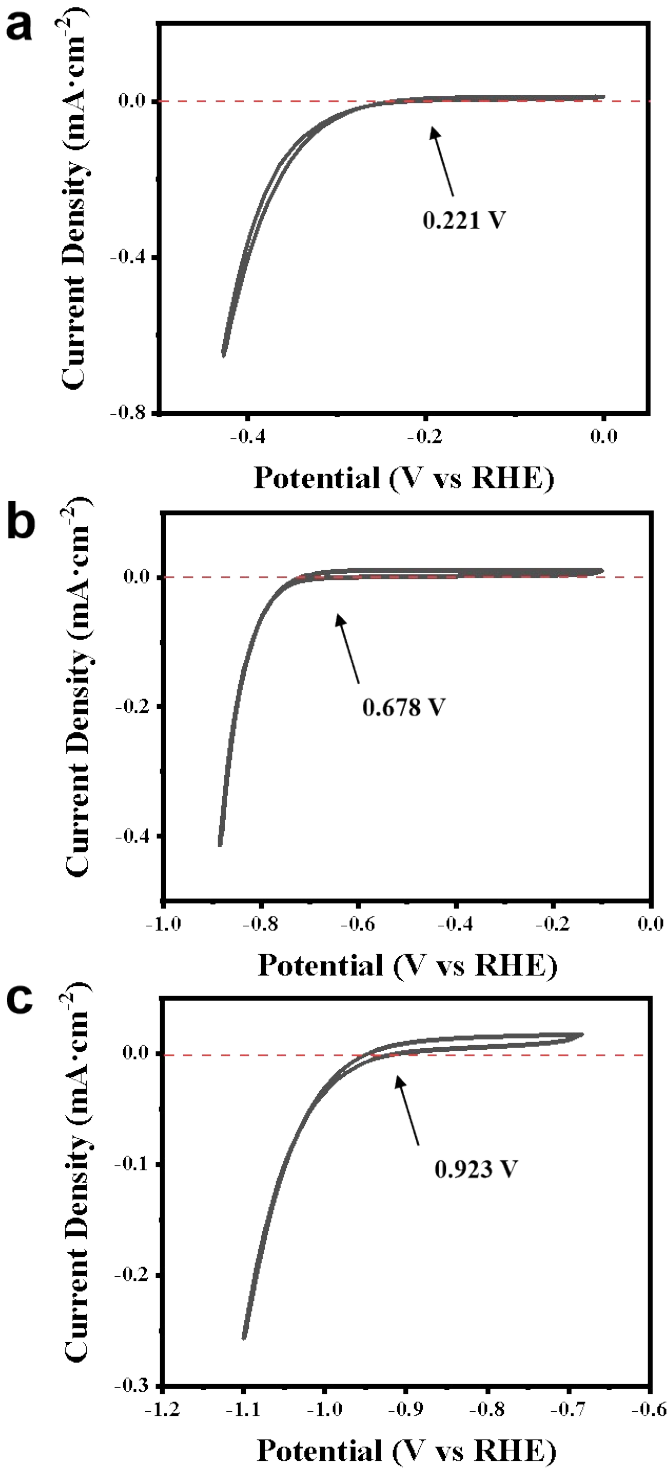

Fig. S36. The calibration curves of the Ag/AgCl electrode (a) and $Hg/HgSO_4$ electrode (b) in 0.5 M H_2SO_4 solution and Hg/HgO electrode (c) in 1.0 M KOH solution.

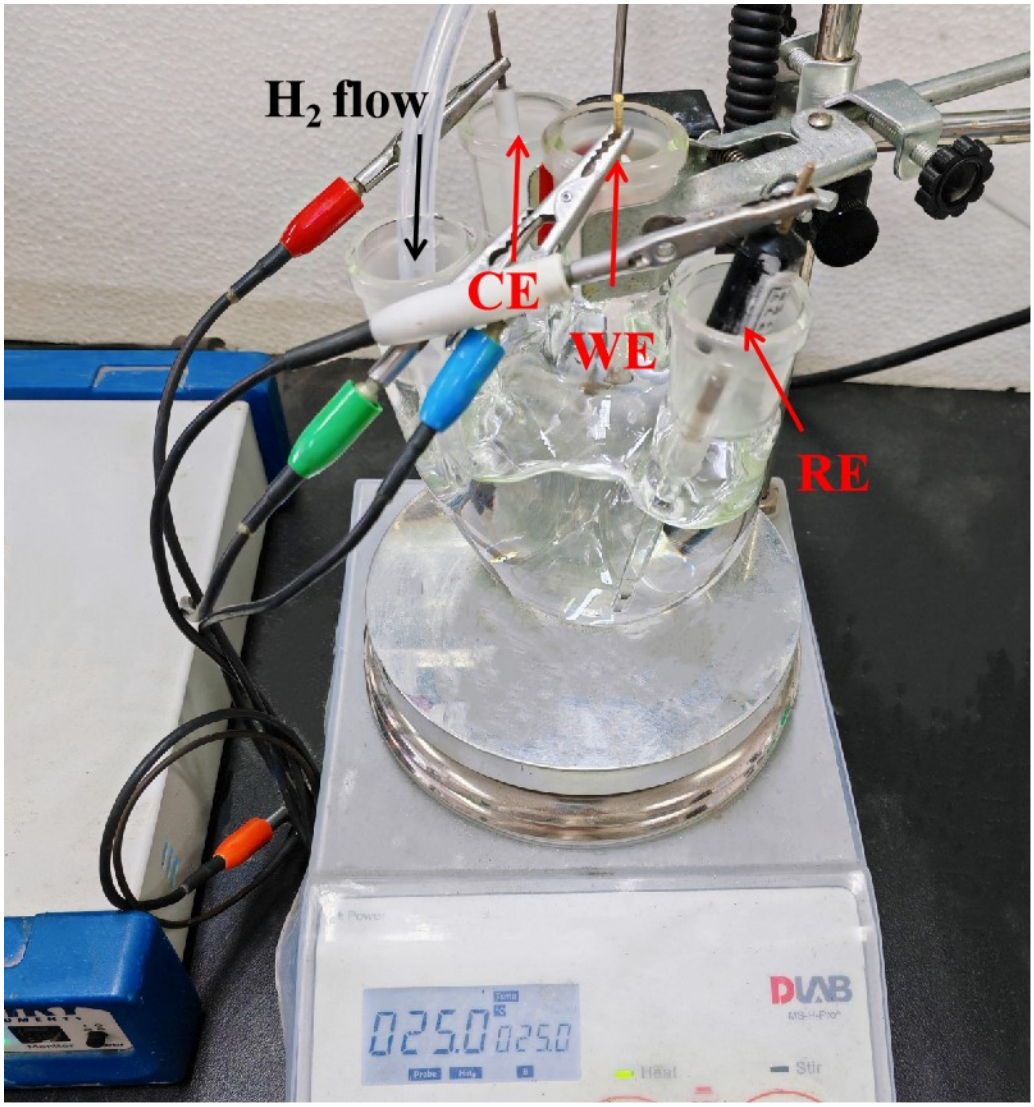

Fig. S37. The calibration setup of the reference electrode.

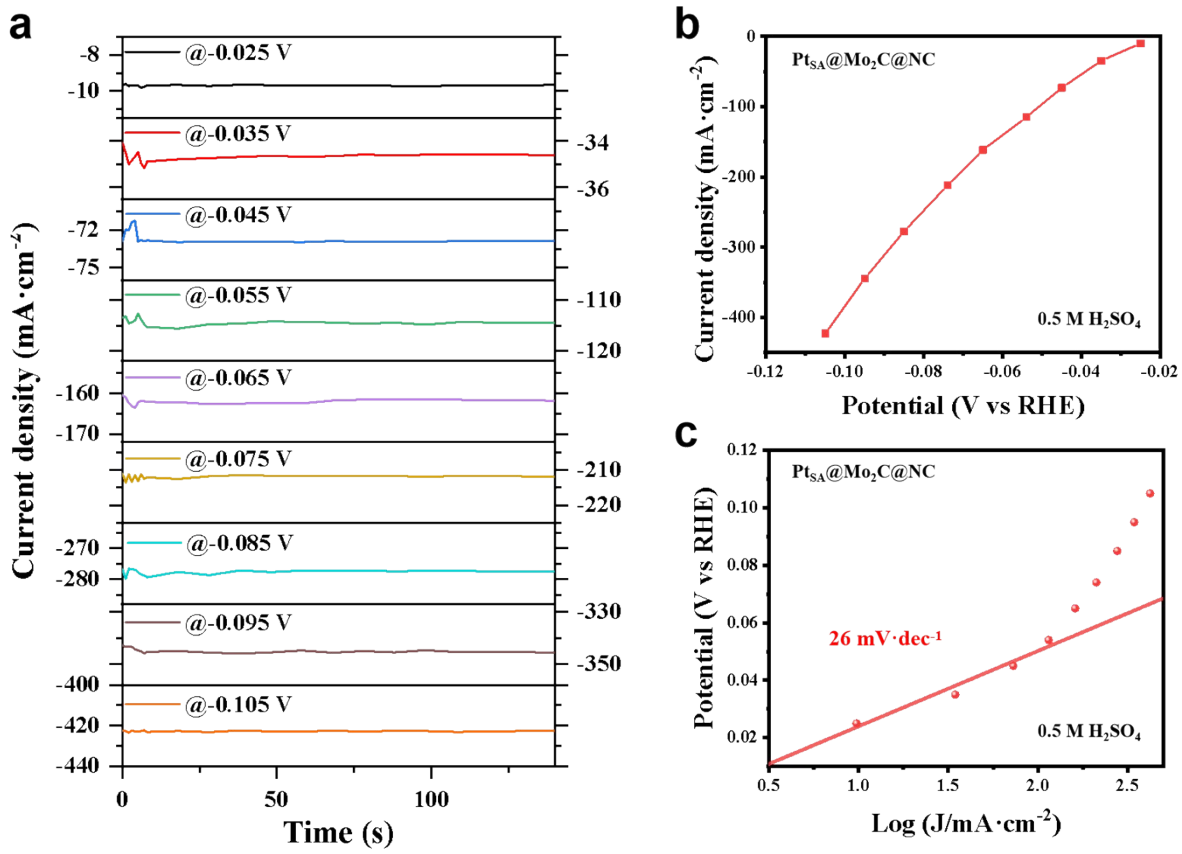

Fig. S38. (a) Chronoamperometry responses of activity stabilized Pt_{SA}@Mo_2C@NC catalyst in 0.5 M H_2SO_4, (b) plot of sampled HER current densities and (c) Tafel plot constructed from steady-state Chronoamperometry responses.

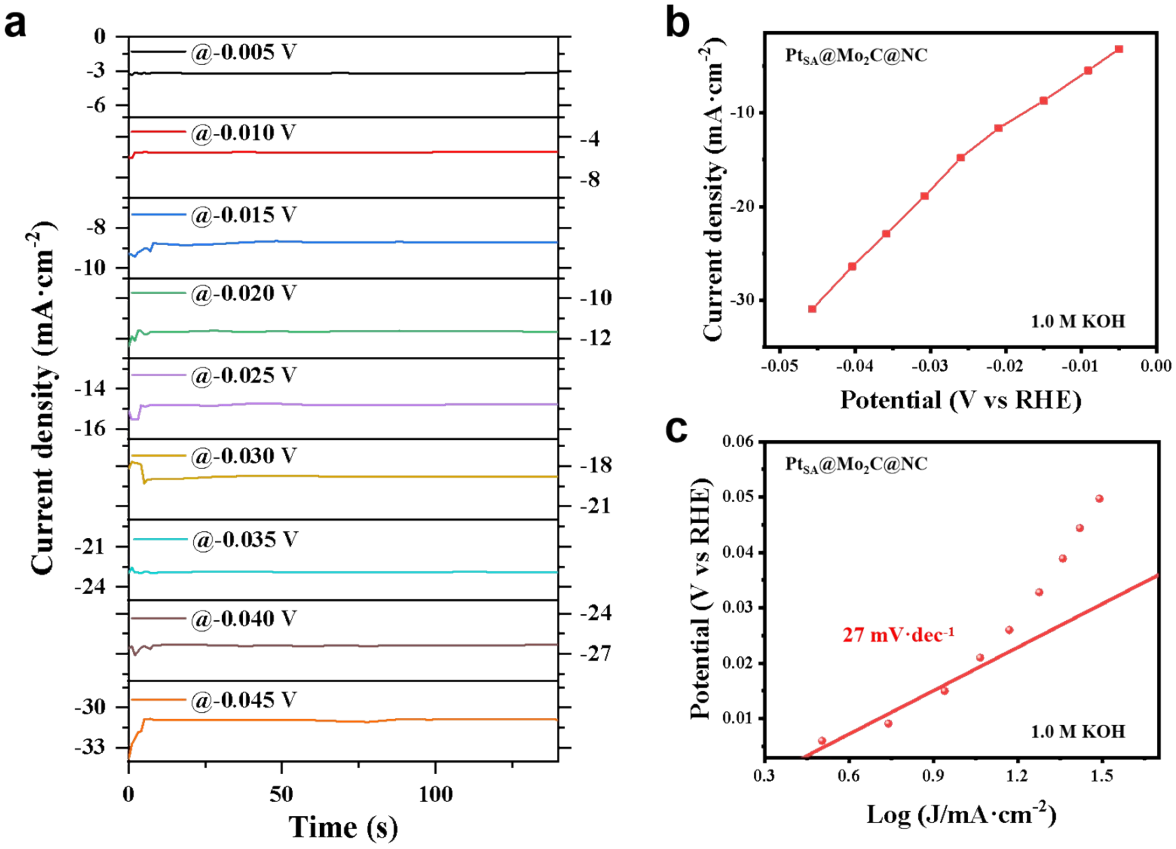

Fig. S39. (a) Chronoamperometry responses of activity stabilized Pt_{SA}@Mo_2C@NC catalyst in 1.0 M KOH, (b) plot of sampled HER current densities and (c) Tafel plot constructed from steady-state Chronoamperometry responses.

Table S1. Zn content of Mo_2C@NC before and after 3M HCl treatment.

Sample	Operation	Zn content (wt%)
Mo_2C@NC	Before 3M HCl	0.05
	After 3M HCl	/

Table S2. Structural parameters extracted from the Pt L_3-edge EXAFS fitting.

Sample	Scattering pair	CN	R(Å)	$\sigma^2(10^{-3}Å^2)$	ΔE_0(eV)	R
Pt_{SA}@Mo_2C@NC	Pt-C	1.61 (7)	2.03 (5)	0.008 (7)	5.5 (4)	0.02
	Pt-N	1.43 (8)	2.56 (5)	0.001 (5)		
	Pt-Mo	1.96	2.75 (3)	0.003 (4)		

Table S3. Comparison of HER performance of Pt_{SA}@Mo_2C@NC with reported electrocatalysts in 0.5 M H_2SO_4.

Electrocatalyst	Tafel slope ($mV \cdot dec^{-1}$)	Overpotential at $100mA \cdot cm^{-2}$ (mV)	References
This work	**14**	**2**	
Pt SASs/AG	29	12	*Energy Environ. Sci.* 2019[1]
Co-substituted Ru	29	13	*Nat. Commun.* 2018[2]
Pt-Cu/Mo_2C	28.2	13	*Nanoscale,* 2020[3]
Pt-ACs/CoNC	27.7	24	*Nat. Commun.* 2022[4]
Mo_2C/CFP-Act	41	37	*J. Catal.* 2020[5]
Pt/TiCO-F	29.7	34	*Adv. Funct. Mater.* 2022[6]
$Ti_3C_2T_x$-Pt_{SA}	45	38	*Nano Lett.* 2022[7]
MAC@Pt 1000	24.95	40	*Small.* 2022[8]
PtCu/WO_3@CF	45.9	41	*Adv. Funct. Mater.* 2022[9]
Pt/TiB_xO_y	32	50	*ACS Catal.* 2022[10]
PtRu@C_2N	31	52	*Chem. Eng. J.* 2022[11]
Ni-Mo_2C@NPC	59	144	*Appli. Catal. B: Environ.* 2021[12]
FD-MoS_2-5	36	164	*Nat Commun.* 2022[13]

Table S4. Comparison of HER performance of Pt_{SA}@Mo_2C@NC with reported electrocatalysts in 1.0 M KOH.

Electrocatalyst	Tafel slope ($mV \cdot dec^{-1}$)	Overpotential at $10mA \cdot cm^{-2}$ (mV)	References
This work	**27**	**2**	
PtRu/mCNTs	33.5	15	*Energy Environ. Sci.* 2022[14]
Pt@CoS	31	28	*Appli. Catal. B: Environ.* 2022[15]
Pt/A-NiCo LDH	38.8	16	*Chem. Commun.* 2022[16]
PtW NWs/C	29	43	*Adv. Energy Mater.* 2022[17]
Pt/X-NCNT	33.3	17	*Adv. Energy Mater.* 2022[18]
NF-Na-Fe-Pt	35.98	31	*Appli. Catal. B: Environ.* 2021[19]
Ni-Mo_2C@NPC	64	183	*Appli. Catal. B: Environ.* 2021[12]
Pt_1-Mo_2C-C	64	155	*J. Energy Chem.* 2021[20]
PtRu@C_2N	63	59	*Chem. Eng. J.* 2022[11]
Pt_{SA}-NiO/Ni	27.07	26	*Nat. Commun.* 2021[21]
Ru@NC	36	26	*Angew. Chem. Int. Ed.* 2018[22]

Table S5. Pt composition of the as prepared catalysts derived from ICP elemental analysis.

Element	$Pt_{SA}@Mo_2C@NC$	$Pt_{NP}@Mo_2C@$ NC	20% Pt/C
Pt	0.93% wt	1.05% wt	20% wt

Table S6. Mass activity of Pt_{SA}@Mo_2C@NC and reference catalysts.

Electrocatalyst	Mass activity ($A \cdot mg_{Pt}^{-1}$)	Overpotential (V)	References
This work	**75.21**	**0.1**	
$Ti_3C_2T_x$-Pt_{SA}	23.21	0.1	*Nano Lett.* 2022[7]
PtCu/WO_3@CF	10.86	0.1	*Adv. Funct. Mater.* 2022[9]
MAC@Pt 1000	1.500	0.1	*Small* 2022[8]
Pt SASs/AG	22.40	0.05	*Energy Environ. Sci.* 2019[1]
Pt-ACs/CoNC	28.6	0.05	*Nat. Commun.* 2022[4]
Pt/MXene	1.847	0.05	*Adv. Funct. Mater.* 2022[23]

Table S7. ICP-OES results of Pt elements before and after 12,000 cycle scans of $Pt_{SA}@Mo_2C@NC$ in 0.5 M H_2SO_4 and 1.0 M KOH solutions.

$Pt_{SA}@Mo_2C@NC$	**0.5 M H_2SO_4**	**1.0 M KOH**
Before HER	0.94% wt	0.94% wt
After HER	0.92% wt	0.93% wt

Table S8. Bader charge and value calculation results of Pt_{SA}@Mo_2C@NC, Pt@Mo_2C and Pt@NC.

Catalyst	Bader charge (e^-)	Value (e^-)
Pt_{SA}@Mo_2C@NC	9.813	0.373
Pt@Mo_2C	9.703	0.593
Pt@NC	9.736	0.528

Reference

1. S. Ye, F. Luo, Q. Zhang, P. Zhang, T. Xu, Q. Wang, D. He, L. Guo, Y. Zhang, C. He, X. Ouyang, M. Gu, J. Liu and X. Sun, *Energy & Environmental Science*, 2019, **12**, 1000-1007.
2. J. Mao, C. T. He, J. Pei, W. Chen, D. He, Y. He, Z. Zhuang, C. Chen, Q. Peng, D. Wang and Y. Li, *Nat Commun*, 2018, **9**, 4958.
3. W. Jia, J. Zhang, Z. Lu, S. Wang and S. Feng, *Nanoscale*, 2020, **12**, 3902-3906.
4. Y. Zhao, P. V. Kumar, X. Tan, X. Lu, X. Zhu, J. Jiang, J. Pan, S. Xi, H. Y. Yang, Z. Ma, T. Wan, D. Chu, W. Jiang, S. C. Smith, R. Amal, Z. Han and X. Lu, *Nat Commun*, 2022, **13**, 2430.
5. J. He, Z. Cui, S. Zhu, Z. Li, S. Wu, L. Zheng, Z. Gao and Y. Liang, *Journal of Catalysis*, 2020, **384**, 169-176.
6. Y. Wu, W. Wei, R. Yu, L. Xia, X. Hong, J. Zhu, J. Li, L. Lv, W. Chen, Y. Zhao, L. Zhou and L. Mai, *Advanced Functional Materials*, 2022, **32**.
7. J. Zhang, E. Wang, S. Cui, S. Yang, X. Zou and Y. Gong, *Nano Lett*, 2022, **22**, 1398-1405.
8. M. Sheng, X. Bin, Y. Yang, Y. Tang and W. Que, *Small*, 2022, **18**, e2203471.
9. L. Liu, Y. Wang, Y. Zhao, Y. Wang, Z. Zhang, T. Wu, W. Qin, S. Liu, B. Jia, H. Wu, D. Zhang, X. Qu, M. Chhowalla and M. Qin, *Advanced Functional Materials*, 2022, **32**.
10. X. Cheng, B. Xiao, Y. Chen, Y. Wang, L. Zheng, Y. Lu, H. Li and G. Chen, *ACS Catalysis*, 2022, **12**, 5970-5978.
11. C. Li, L. Zhang, Y. Zhang, Y. Zhou, J. Sun, X. Ouyang, X. Wang, J. Zhu and Y. Fu, *Chemical Engineering Journal*, 2022, **428**, 131085.
12. Y. Lu, C. Yue, Y. Li, W. Bao, X. Guo, W. Yang, Z. Liu, P. Jiang, W. Yan, S. Liu, Y. Pan and Y. Liu, *Applied Catalysis B: Environmental*, 2021, **296**.
13. J. Xu, G. Shao, X. Tang, F. Lv, H. Xiang, C. Jing, S. Liu, S. Dai, Y. Li, J. Luo and Z. Zhou, *Nature Communications*, 2022, **13**, 2193.
14. B. Pang, X. Liu, T. Liu, T. Chen, X. Shen, W. Zhang, S. Wang, T. Liu, D. Liu, T. Ding, Z. Liao, Y. Li, C. Liang and T. Yao, *Energy & Environmental Science*, 2022, **15**, 102-108.
15. A. Mosallanezhad, C. Wei, P. Ahmadian Koudakan, Y. Fang, S. Niu, Z. Bian, B. Liu, T. Huang, H. Pan and G. Wang, *Applied Catalysis B: Environmental*, 2022, **315**, 121534.
16. B. Fan‡, H. Wang‡, X. Han, Y. Deng and W. Hu, *Chemical Communications*, 2022, **58**, 8254-8257.
17. L. Gao, Z. Yang, T. Sun, X. Tan, W. Lai, M. Li, J. Kim, Y.-F. Lu, S.-I. Choi, W. Zhang, C. Ma, S. C. Smith, Y.-G. Zhou and H. Huang, *Advanced Energy Materials*, 2022, **12**, 2103943.
18. W. Yu, H. Huang, Y. Qin, D. Zhang, Y. Zhang, K. Liu, Y. Zhang, J. Lai and L. Wang, *Advanced Energy Materials*, 2022, **12**, 2200110.
19. Y. Zhao, Y. Gao, Z. Chen, Z. Li, T. Ma, Z. Wu and L. Wang, *Applied Catalysis B: Environmental*, 2021, **297**, 120395.
20. S. Niu, J. Yang, H. Qi, Y. Su, Z. Wang, J. Qiu, A. Wang and T. Zhang, *Journal of Energy Chemistry*, 2021, **57**, 371-377.
21. K. L. Zhou, Z. Wang, C. B. Han, X. Ke, C. Wang, Y. Jin, Q. Zhang, J. Liu, H. Wang and H. Yan, *Nature Communications*, 2021, **12**, 3783.
22. Z.-L. Wang, K. Sun, J. Henzie, X. Hao, C. Li, T. Takei, Y.-M. Kang and Y. Yamauchi, *Angewandte Chemie International Edition*, 2018, **57**, 5848-5852.
23. Y. Wu, W. Wei, R. Yu, L. Xia, X. Hong, J. Zhu, J. Li, L. Lv, W. Chen, Y. Zhao, L. Zhou and L. Mai, *Advanced Functional Materials*, 2022, **32**, 2110910.